

The constant beat: cardiomyocytes adapt their forces by equal contraction upon environmental stiffening

Nils Hersch, Benjamin Wolters, Georg Dreissen, Ronald Springer, Norbert Kirchgeßner*, Rudolf Merkel and Bernd Hoffmann[†]

Institute of Complex Systems, ICS-7: Biomechanics, Forschungszentrum Jülich GmbH, 52425 Jülich, Germany

*Present address: Institute of Agricultural Sciences, ETH Zürich, Universitätsstraße 2, 8092 Zürich, Switzerland

[†]Author for correspondence (b.hoffmann@fz-juelich.de)

Biology Open 2, 351–361
doi: 10.1242/bio.20133830
Received 13th December 2012
Accepted 23rd December 2012

Summary

Cardiomyocytes are responsible for the permanent blood flow by coordinated heart contractions. This vital function is accomplished over a long period of time with almost the same performance, although heart properties, as its elasticity, change drastically upon aging or as a result of diseases like myocardial infarction. In this paper we have analyzed late rat embryonic heart muscle cells' morphology, sarcomere/costamere formation and force generation patterns on substrates of various elasticities ranging from ~1 to 500 kPa, which covers physiological and pathological heart stiffnesses. Furthermore, adhesion behaviour, as well as single myofibril/sarcomere contraction patterns, was characterized with high spatial resolution in the range of physiological stiffnesses (15 kPa to 90 kPa). Here, sarcomere units generate an almost stable contraction of ~4%. On stiffened substrates the

contraction amplitude remains stable, which in turn leads to increased force levels allowing cells to adapt almost instantaneously to changing environmental stiffness. Furthermore, our data strongly indicate specific adhesion to flat substrates via both costameric and focal adhesions. The general appearance of the contractile and adhesion apparatus remains almost unaffected by substrate stiffness.

© 2013. Published by The Company of Biologists Ltd. This is an Open Access article distributed under the terms of the Creative Commons Attribution Non-Commercial Share Alike License (<http://creativecommons.org/licenses/by-nc-sa/3.0>).

Key words: Cardiomyocyte, Traction force microscopy, Cell adhesion, Mechanoresponse, Myofibril, Sarcomere

Introduction

Mechanical properties of tissues strongly affect embedded mammalian cells. The consequences extend from simple, small adaptations of rather isolated cellular structures all the way to initiation of very complex differentiation pathways. One of the most potent mechanical signals is the elasticity of the environment. Various cell types respond with simple reinforcements of adhesion and cytoskeletal structures upon substrate stiffening (Giannone et al., 2003; Krishnan et al., 2009). More extensive adaptations have been described for elasticity dependent stem cell differentiation. Here, cell fate could be directed by substrate stiffness in direction of neuronal, bone or muscle progenitors (Discher et al., 2009; Engler et al., 2006). In addition, various other cell types undergo further differentiation processes after environmental stiffening without changing their tissue localization. Prominent examples can be found in mammalian heart myocardial tissue, especially during aging and after infarction or other coronary heart diseases (Herrmann et al., 2003; Hinz, 2009; Koltai et al., 1984; Mazhari et al., 2000). While elasticities of healthy myocardial tissues range from 10 to 30 kPa, stiffnesses in heart stroke affected areas increase to values of up to 150 kPa (Berry et al., 2006; Gupta et al., 1994; Jacot et al., 2010). Triggered by this stiffening myocardial fibroblasts differentiate together with bone marrow stem cells into myofibroblasts, leading to scar tissue formation with drastic changes of myocardial physical properties. Differentiation

processes of those cells go along with extensive functional changes. In contrast, myocardial embedded cardiomyocytes, responsible for the regular heartbeat, do not seem to adapt morphologically and functionally to such environmental changes.

Cardiomyocytes of healthy myocardial tissue interact mechanically with their environment via costameric adhesions to surrounding extracellular matrix molecules (ECM) and via cell–cell contacts at intercalated disks to other myocytes. In disease affected tissues adhesion structures of cardiomyocytes become remodeled. As a consequence, adhesion sites of cardiomyocytes increase at sites of scar formation to the ECM as well as to non-spontaneously contracting cells like endothelial cells or myofibroblasts (van den Borne et al., 2010). Resulting changes in adhesion and heart tissue elasticity can affect the volume of blood filling the heart and therefore also the stroke volume according to the Frank–Starling mechanism and the force–velocity relation (Fukuda et al., 2001; Martyn and Gordon, 2001; Rassier and Pavlov, 2010). Elevated heart load goes along with enhanced forces during cardiomyocyte contraction due to cell stretching and therefore increased sarcomere lengths as force generating subunit of myofibrils from originally ~1.9 µm to extended lengths of up to 2.4 µm (Rassier and Pavlov, 2010).

Even isolated neonatal cardiomyocytes recognize substrate elasticity as very potent signal inducing maturation and functional development. This was shown, for example, examining cells grown on substrates mimicking the natural

elasticity of ~ 10 kPa and on stiffer ones (50 kPa). In the latter case sarcomere alignment was reduced in comparison to the former. Additionally, cellular forces were reported to be highest on 10 kPa substrates and reduced on softer and stiffer materials (Jacot et al., 2008; Jacot et al., 2010). For neonatal cardiomyocytes grown on elastomeric micropillars, twitch forces increased on stiffened posts while twitch velocities leveled down. Elevated forces were accompanied by increased sarcomere lengths and z-band widths (Rodriguez et al., 2011). Other studies indicate that beating frequency and fraction of isolated cardiomyocytes corresponded best to natural characteristics on substrates resembling native myocardial elasticities (Bajaj et al., 2010; Engler et al., 2008). Remarkably, several aspects of how cardiomyocytes respond to substrate elasticity are still under debate since other studies indicate a complete loss of myofibrils on soft 1 kPa substrates (Bajaj et al., 2010), an elevated number of beating myocytes after maturation on very soft substrates (below 1 kPa) (Shapira-Schweitzer and Seliktar, 2007) or increasing force values upon substrate stiffening to up to 144 kPa (Bhana et al., 2010). Furthermore, atomic force microscopy measurements indicate a completely unaffected cell elasticity of cardiomyocytes on substrate elasticities ranging from 8 to 50 kPa (Shi et al., 2011).

After isolation from tissue and growth as isolated cells on flat substrates myocytes display an altered adhesion pattern (Hilenski et al., 1992; Simpson et al., 1993). This adaptation includes reorganization of costameric structures, resulting in adhesive sites that are structurally similar to focal adhesions (FA), which are typically found in non-muscle cells (Decker et al., 1990). Simultaneously, intercalated disks at the end of myofibrils remodel to adherens junctions as well as to FA like structures. All these structures provide strong adhesion sites responsible for mechanical communication between the ECM and the contractile machinery of the cultured cells (Goncharova et al., 1992; Simpson et al., 1993). The disassembly of the contractile apparatus upon isolation and a reassembly from pre-myofibrils after attachment to cell culture substrates seem to be decisive for this environmentally controlled adaptation (Du et al., 2003; Sanger et al., 2005).

Previous work has shown that both environmental stretch and cell contractility increase size and frequency of adhesion structures (Miller et al., 2000; Sharp et al., 1997; Simpson et al., 1993). Furthermore, in early work Danowski and co-workers cultivated adult cardiomyocytes on a thin and flexible silicone membrane and observed pleat-like wrinkles with a spacing of ~ 1.9 μm (Danowski et al., 1992). Pleats coincided with the distribution and distance of z-disks. These observations clearly indicated the transmission of mechanical force at sites of costameric adhesions. Later traction force microscopy measurements were evaluated with the assumption that forces were exclusively applied at FAs at the ends of myofibrils and stress fibers. These analyses resulted in force values of ~ 15 nN per FA and force dipole values in the 6 pNm range (Balaban et al., 2001; Cesa et al., 2007). The force dipole, also called generalized first moment, is just the sum of the scalar products of the vectors force and its position. For a cell of the size of a cultivated cardiomyocyte a force dipole of 6 pNm roughly corresponds to overall contractile forces in the 200 nN range.

Although cardiomyocytes have been intensively analyzed for more than 20 years, several important questions are still not yet answered. For example, it is not entirely clear how neonatal

cardiomyocytes adhere during maturation or how and where remodeled adhesion sites transmit traction forces. Adaptations in morphology, structure and composition of adhesion structures to substrate elasticity are also not fully elucidated. In this paper we have addressed these important questions of adhesion behavior and force generation/transmission of rat late embryonic cardiomyocytes. Cells were grown on well-characterized silicone rubber substrates of various elasticities in the natural range. Traction force measurements were performed and analyzed in depth using two independent algorithms. Special care was taken to achieve high spatial resolution to determine the forces transmitted at every single putative adhesion structure. Moreover, the local contractile strain along single myofibrils was determined.

In summary our data prove that cultured late embryonic rat cardiomyocytes exhibit very stable contraction amplitudes of sarcomeric units along separate myofibrils. This behavior generates increased force values upon substrate stiffening. At all substrate elasticities analyzed adhesion and force transmission occur along the whole length of myofibrils at sites of costameres and at remodeled myofibril ends. Interestingly, in the physiological elasticity range substrate stiffness did not affect the lengths of relaxed or contracted sarcomeric units. This is not in agreement with the Frank–Starling mechanism and indicates that, despite it being well established in tissue, various regulatory mechanisms connected with this mechanism might be incompletely active in isolated cardiomyocytes.

Results

The sarcomeric force generation system is formed independently of environmental elasticity

In order to analyze contractile and adhesive behavior of cardiomyocytes in an elasticity range of ~ 1 to 500 kPa silicone rubber substrates were fabricated. In a first step, late embryonic myocytes were grown for three days on substrate elasticities spanning the physiological range of 15 to 150 kPa and, additionally, on artificially very soft (~ 1 kPa) or very stiff substrates (500 kPa) and analyzed for differences in cell shape. When grown on substrate elasticities of 15 kPa and stiffer a large percentage of cells were characterized by a shape index *si* below 0.8, corresponding to a more angular shape (Fig. 1A,B). Just 30% of all cells exhibited a roundish, mostly convex shape (*si* above 0.8). On very stiff substrates almost all cells were angular in shape (fraction of roundish cells below 10%). Only on very soft substrates (~ 1 kPa) the ratio between round and angular shaped myocytes was basically inverted with $\sim 80\%$ of cells exhibiting a convex outline (Fig. 1A,B).

Since edge curvature depends on the mechanical stress formed within the network of inner actin fibers (Bischofs et al., 2009), we analyzed whether sarcomeres, the force generating units of myocytes, were differently formed or organized depending on substrate stiffness. To this end we used α -actinin as marker protein (Fig. 2). Interestingly, myocytes always displayed regularly striated myofibrils irrespective of substrate elasticity (~ 1 kPa to 500 kPa). This observation was confirmed with actin as marker (Fig. 2) indicating that the whole force generating system is functional and largely unaffected by changes in environmental elasticity. More elaborate analyses of myofibril formation within the most relevant physiological range of substrate elasticities between 15 and 90 kPa revealed that neither the number of costameres per cell, nor the mean area per α -actinin cluster or the fraction of the cell area labeled by α -actinin was significantly affected by substrate elasticity (Fig. 3).

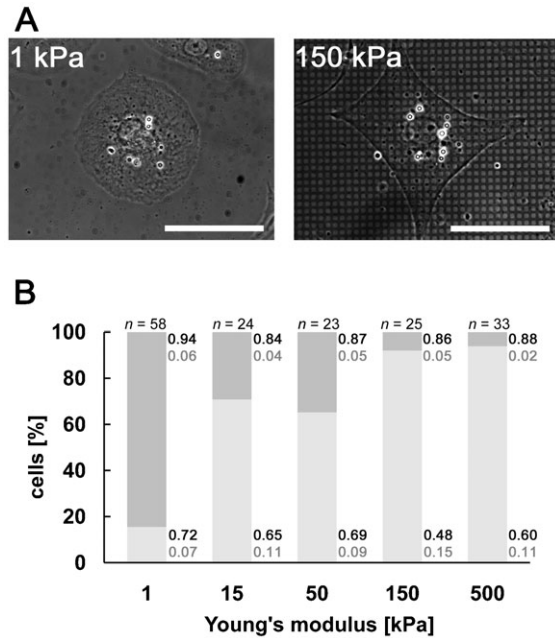


Fig. 1. Substrate elasticity dependent cell shape adaptation of myocytes. Freshly isolated rat cardiomyocytes were incubated for 3 days on silicone rubber substrates ranging in their elasticity from ~ 1 to 500 kPa as given. Subsequently, cells were analyzed for either round (shape index, $si > 0.8$) or elongated, angular ($si \leq 0.8$) cell shape (A) using image processing. Left micrograph $si = 0.96$, right micrograph $si = 0.45$. Scale bars: 50 μm . Distribution between both shapes is given in B. Round cell shape = dark grey and elongated shaped cells = light grey. n = number of analyzed cells. Mean values (black) including s.d. (grey) of shape indices for round and elongated cells are given next to the bars.

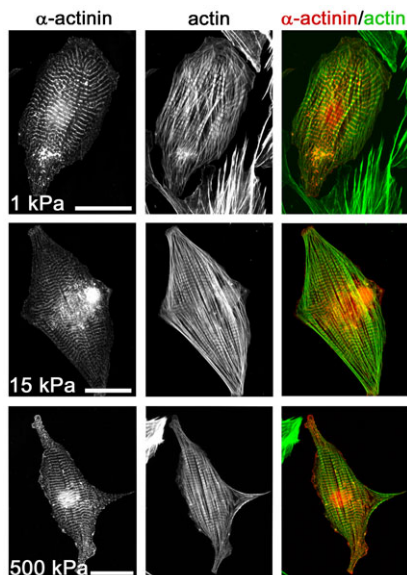


Fig. 2. Stable formation of the force generating system of myocytes. Cardiomyocytes were grown on ~ 1 kPa, 15 kPa and 500 kPa stiff elastomeric substrates for 3 days and analyzed after fixation for myofibril formation using α -actinin (left) and actin (middle) as marker proteins. Overlay images are given (right). Scale bars: 50 μm .

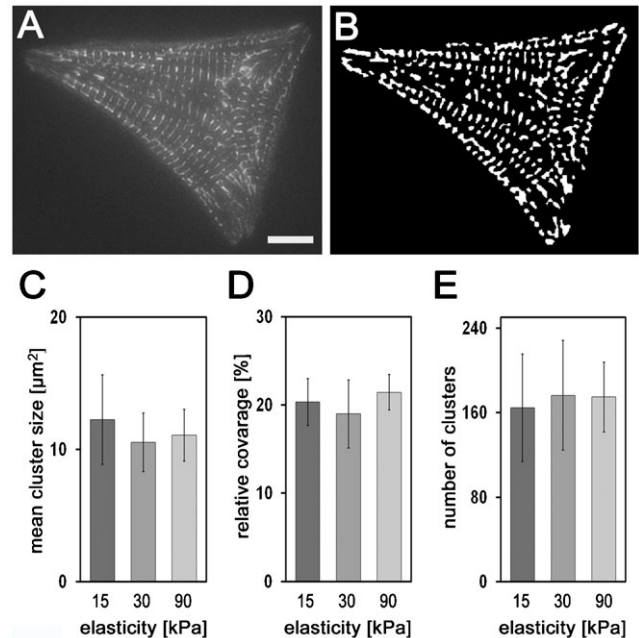


Fig. 3. Substrate elasticity independent formation of costameres. GFP- α -actinin transfected cells (A) were grown for 3 days on 15 kPa, 30 kPa and 90 kPa substrates. Live cell images were segmented using image processing (B). Scale bar: 10 μm . Mean α -actinin cluster size (C), relative coverage of cells with α -actinin clusters (D) and the total number of α -actinin clusters per cell (E) were determined. All results are indicated with their respective s.d.; $n = 16$ cells for 15 kPa, 20 cells for 30 kPa and 13 cells for 90 kPa.

With respect to the cytoskeleton, the only effect observed on artificially soft ~ 1 kPa substrates was a slightly reduced order and alignment of individual myofibrils with respect to each other. Since reduced order of myofibrils might indicate an altered coupling of costameres to intracellular structures and also to the outer environment, we additionally analyzed the localization of plectin. This protein is vital for the mechanical coupling of sarcomeric borders (z-bands) to the intermediate filament protein desmin and, via this link, for the coupling between myofibrils and the whole dystrophin/glycoprotein complex embedded in the plasma membrane (Konieczny et al., 2008). These analyses revealed a localization of plectin at sites of sarcomere separating z-bands on all substrate elasticities tested. Interestingly, while two distinct small plectin spots were found on both sides of z-bands on ~ 1 kPa, these spots visibly enlarged in size in an elasticity dependent manner (Fig. 4A). This structural reinforcement resulted in plectin signals co-localizing with actin along its full sarcomeric length on stiff 500 kPa substrates.

The structural studies performed above suggest a functional force generation system as well as a proper connection of myofibrils to the plasma membrane. However, whether plasma membrane connected costameres also interacted with the extracellular matrix was still unclear. We therefore cultivated myocytes on substrates with elasticities from ~ 1 kPa to 500 kPa and stained them for vinculin as marker for FA as well as for integrin-dependent costamere linked adhesion sites. As shown in Fig. 4B, these micrographs display distinct signals at both ends of every single myofibril. Furthermore, vinculin co-localized with costameres. These signals were variable in intensity between individual cells and slightly blurred on very soft substrates.

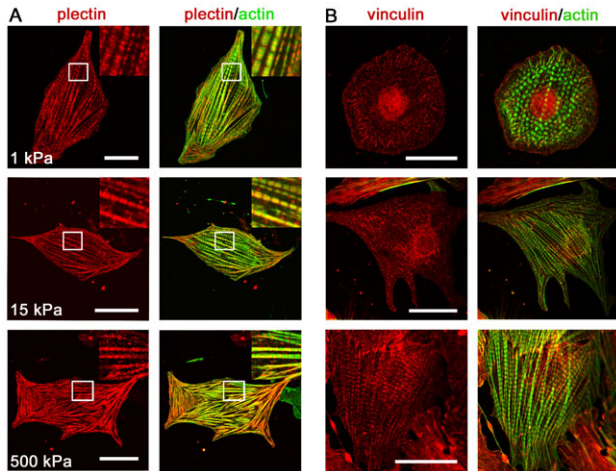


Fig. 4. Myofibril alignment and plasma membrane attachment. Cardiomyocytes were grown for 3 days on substrates of indicated elasticities. Subsequently, cells were fixed and stained for plectin and actin (A) or vinculin and actin (B). Insets in A show enlargements of the areas within the white squares. Note the elasticity dependent reinforcement of plectin and vinculin around sites of z-bands. Scale bars: 20 μm .

Nevertheless, these vinculin stainings might argue for an interaction with integrin, and therefore with the environment, at sites of costameres on each substrate elasticity tested.

Force is transmitted at sites of costameric and focal adhesions. To further test the adhesive behavior of cardiomyocytes, traction force microscopy was performed on spontaneously contracting GFP- α -actinin transfected cells grown on 15 kPa, 30 kPa, and 90 kPa stiff substrates (see also supplementary material Movie 1). Here, force calculation was based on the assumption of point forces acting at interactively chosen adhesion sites. From the forces determined in this way substrate deformation fields were back calculated (Fig. 5, top) and compared with the actual measured displacements. From those calculations residual displacements for each tracked marker could be constructed. Whenever exclusively FAs were chosen as force induction points major residual displacements remained present below the center of cells (Fig. 5B,E). Vice versa, choosing only costameres as force induction points resulted in back calculated displacements that fitted the measured ones well below the interior of the cell while major residuals remained at the periphery. (Fig. 5C,E). Only combining FAs and costameres resulted in low residual displacements over the whole field (Fig. 5D,E).

As additional control we identically analyzed similar traction force experiments on myofibroblasts, a cell type well known to adhere exclusively via FAs with strong contractile stress fibers in between. Whenever we used as force induction points either FAs alone (Fig. 5G,J), or together with them a fictitious pattern, similar to the ones used in myocytes for costameres, along stress fibers (Fig. 5I,J), we found very low residual displacements. In contrast, high residual displacements resulted if exclusively points along stress fibers were used (Fig. 5H,J). Interestingly, for this cell type combining all types of force induction points was not further reducing the residual displacements. Thus our implementation of traction force microscopy was well able to discriminate between the different modes of force application. Taken together, these data clearly prove the simultaneous

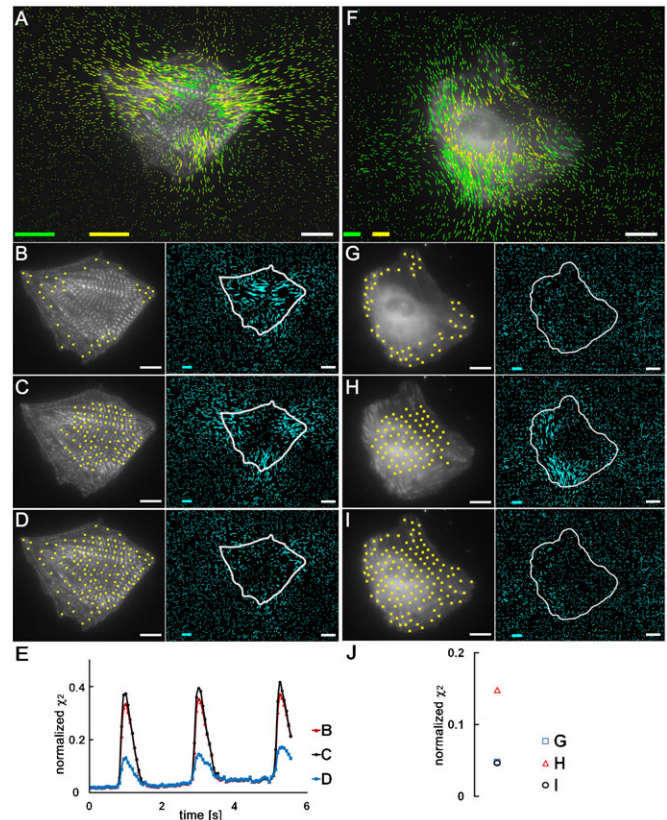


Fig. 5. Costameric and focal adhesion dependent traction forces of myocytes. GFP- α -actinin transfected cardiomyocytes (A–E) and GFP-VASP transfected myofibroblasts (F–J) were grown on fluorescent bead micropatterned 15 kPa (exemplarily shown here), 30 kPa and 90 kPa elastomeric substrates. Spontaneously contracting myocytes were analyzed by live cell microscopy to visualize the substrate deformation field (A, green arrows) upon contraction. Using interactively chosen force induction points and elasticity theory cell forces (not shown) and the resulting back calculated substrate deformations (A, yellow arrows) were determined for each time point. As result we received a residual displacement vector for each marker bead (B–D, right, blue arrows). Choosing as force induction points (yellow squares) either FAs only (B), costameres only (C) or both together (D) back calculations reproduced the actual deformation field with very different accuracy. Frame rate = 17 Hz. As control, measured substrate deformations and back calculated substrate deformations of stably adhered myofibroblasts (F) were determined as described for myocytes using FAs (G), a lattice mimicking the length of two sarcomeres ($\sim 4 \mu\text{m}$) along stress fibers (H) and both (I) as force induction points. Here, for displacement calculation an image of the same substrate area was taken after cell removal. For each back calculation the normalized squared deviation (χ^2) between fit result and measured data was determined as exemplarily given in E,J. Note that for myocytes residual deformations are low only if both FAs and costameres are taken as force induction points, while for myofibroblasts FAs alone are fully sufficient. Scale bars for displacements (yellow and green) in A,F: 0.5 μm ; for the cell size (white): 10 μm ; and for residual deformation (light blue): 0.2 μm .

adhesion and force transmission of cardiomyocytes at sites of FAs and costameres.

Force generation increases with substrate stiffening

Based on the results given above we evaluated the sum of all contractile forces of GFP- α -actinin transfected cells using either both FAs and costameres as force induction points or, alternatively, a hexagonal lattice of fictitious points with a lattice constant of 5 μm , covering the whole area of the cell (Fig. 6A,B). The latter choice was necessary to increase the

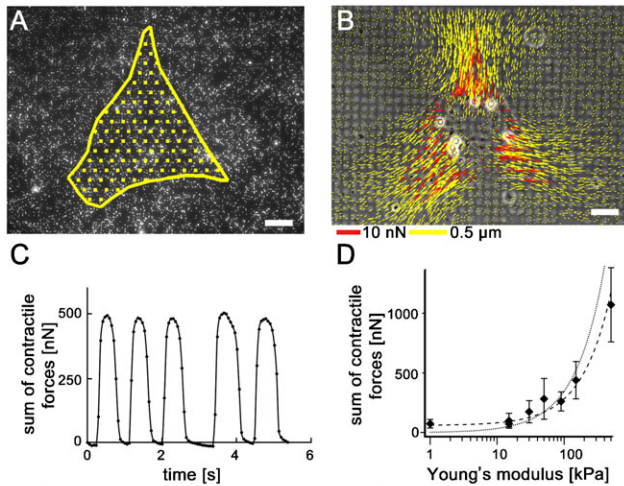


Fig. 6. Stiffness dependent force generation of myocytes. After growth of myocytes for 3 days on bead micropatterned substrates (A) with elasticities ranging from ~ 1 to 500 kPa (D), traction force microscopy was performed on spontaneously contracting cells. Applying elasticity theory based on substrate deformations (B, yellow arrows) with a hexagonal grid used as force induction points (A), forces per grid point (B, red arrows) were determined for every image of the time stack. Scale bars: 10 μm . The time course of the sum of all contractile forces for the exemplarily given cell is indicated (C). Maximum values of the sum of all contractile forces were averaged for all cells per substrate elasticity and are indicated with the respective s.d. in D using a logarithmic substrate stiffness scale. The dotted curve displays a fitted proportional force increase. The dashed curve indicates a fitted linear force increase. $n \geq 15$ cells per elasticity.

number of analyzable cells since transfection rates of vital myocytes are always very low. On all substrate elasticities tested both methods revealed highly comparable contractile forces with surprisingly small differences (Table 1). We therefore analyzed cell forces of single myocytes on substrate elasticities in the range of ~ 1 to 500 kPa using point forces on such a hexagonal grid. Independent of substrate elasticity, data prove stable spontaneous myocyte contractions over time (Fig. 6C). In good agreement with former analyses (Jacot et al., 2008), these data revealed low force generation of myocytes grown on soft substrates (Fig. 6D; supplementary material Fig. S1A). With increasing stiffness, contractile forces rose continuously from values of only 10 nN (s.d. 36 nN, $n=22$) on ~ 1 kPa substrates to more than 800 nN (s.d. 311 nN, $n=14$) on 500 kPa stiff substrates. Within the physiological range from 15 to 150 kPa this increase was almost linear. Increasing contractile forces upon substrate stiffening went along with unchanged average contraction frequencies, with 38 (s.d. 18) spontaneous contractions per minute on soft (~ 1 to 15 kPa, $n=30$ cells) and 36 (s.d. 18) on stiff (150 to 500 kPa, $n=30$ cells) substrates.

In cell force retrieval algorithms based on force fields the complete interface between cell and substrate is used as putative force induction area. Here, the same elasticity dependent increase of generated cell forces was found albeit with slightly different absolute values (Fig. 7D; supplementary material Fig. S1B). Furthermore, substrate deformation and force fields of GFP- α -actinin transfected cells (Fig. 7A) were not just localized mainly at FA positions but also along most parts of myofibrils independent on substrate elasticity (Fig. 7B,C). These data confirm once more that adhesion of myocytes occurs simultaneously at FAs and costameres.

Contractions of separate myofibril sarcomeric units are stable Elevating force values on stiffening substrates with a virtually unaffected cell force generating system opened the possibility of elasticity adapted contractile amplitudes of myofibrils. If this increase in force was based on a Frank–Starling like mechanism, it should be accompanied by elasticity dependent sarcomere lengths and contractions (de Tombe et al., 2010; Hanft et al., 2008). For this reason we analyzed the contraction patterns of discrete myofibrils over several contractions (exemplarily shown in Fig. 8A). This was done for cells grown on substrates spanning the most relevant natural elasticity range of 15 to 90 kPa.

For every myofibril we could identify a central spot that barely moved during contraction (Fig. 8B,C, black arrowhead). On both sides GFP- α -actinin labeled z-bands displaced upon contraction towards the myofibril center. This z-band displacement along the filament (Fig. 8C) revealed a stable contractile strain, i.e. relative shortening, for about the central half of each myofibril. As contractions sum up along the fibril this corresponds to a linearly increasing displacement of the more outside located sarcomeres within the inner part of myofibrils (Fig. 8B,C). Interestingly, displacements of outmost sarcomeric units often leveled down to a plateau like displacement caused most likely by simple transmission of inner myofibril displacement without additional contractility (Fig. 8C).

In order to characterize the exact contractile behavior of discrete myofibrils, we automatically detected the linear region of each displacement-position curve. Within this region a line was fitted to the displacements. The slope of this line is the contractile strain (relative shortening) of the myofibril (see Materials and Methods). Averaging slope values of 2 to 4 independent myofibrils per cell characterized its mean myofibril contractile behavior (Fig. 8D). Mean values for various cells grown on 15 kPa, 30 kPa or 90 kPa revealed a large spread in cell averaged myofibril contractile strain between 2% and 8% for 15 kPa substrates ($n=7$ cells with 15 myofibrils), 2% and 12% for 30 kPa substrates ($n=13$ cells with 29 myofibrils) and 1% and 6% for 90 kPa substrates ($n=8$ cells with 20 myofibrils) (Fig. 8D). However, with contraction values of $\sim 4\%$ (4.7% s.d. 2.1% for 15 kPa, 4% s.d. 2.9% for 30 kPa, 3% s.d. 1.7% for

Table 1. Comparison of the averaged sum of all contractile cell forces using either FA and costameres or alternatively a hexagonal lattice as force induction points for cells grown on 15, 30 and 90 kPa stiff substrates. s.d. is given in parentheses. n indicates number of cells analyzed.

Elasticity [kPa]	FA+costamer [nN]	Hexagonal lattice [nN]	Difference [%]
15 $n=16$	74 (24)	74 (26)	3.9 (8.4)
30 $n=20$	174 (94)	175 (93)	2.3 (1.9)
90 $n=13$	262 (82)	261 (80)	2.3 (3.3)

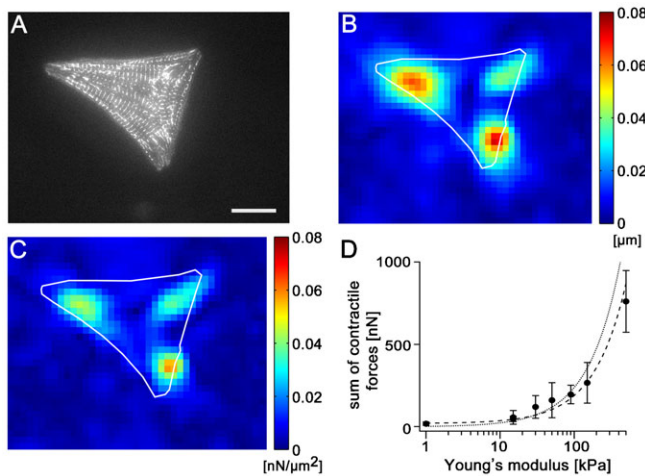


Fig. 7. Force fields along the contractile apparatus. GFP- α -actinin transfected myocytes (A) were grown for 3 days on bead micropatterned substrates with elasticities as indicated in (D). Substrate deformation fields were determined (B) and entire force fields were retrieved (C). Scale bar: 10 μ m. The sum of all maximum contractile forces were averaged over all cells analyzed per substrate elasticity and are indicated with the respective s.d. in D using a logarithmic substrate stiffness scale. The dotted curve displays a fitted proportional force increase. The dashed curve indicates a fitted linear force increase. $n \geq 20$ cells per elasticity.

90 kPa, Fig. 8D) overall averaged myofibril contractile strains showed no significantly different values for all substrate elasticities analyzed. Notably, substrate elasticity did also not influence sarcomeric length for the inner myofibril region. No matter which elasticity was analyzed, contraction started from basically identical sarcomeric lengths of 1.9 μ m in relaxed state (s.d. 0.13 μ m for 15 kPa, s.d. 0.17 μ m for 30 kPa, s.d. 0.11 μ m for 90 kPa).

These data clearly point to a morphological and functional highly stable myofibril contractile mechanism that is basically unaffected and robust against changes in environmental stiffness.

Discussion

Cardiomyocytes are the mechanically most active cell type in mammals. Over decades these cells pump almost constant volumes of blood although environmental conditions within the myocard can change drastically. For example, the molecular composition of the extracellular matrix and the relative amounts of cell types populating it change substantially during embryogenesis, aging or diseases like heart strokes. Most of these changes go along with alterations in tissue elasticity causing stiffening from elasticities in the 10 kPa range found for healthy young myocard to values of up to 100 kPa and sometimes even higher (Berry et al., 2006; Gupta et al., 1994; Jacot et al., 2008).

In light of this background it is even more surprising that cardiomyocytes are morphologically and functionally barely affected by substrate elasticity. In the present study we could clearly show that myocytes from late rat embryos form contractile myofibrils by a very stable mechanism. These fibrils are not visibly affected in number, length or regularity of striation when cells are grown on elastomeric substrates with stiffnesses covering the complete natural range. Even extreme elasticity values of very soft \sim 1 kPa or very stiff 500 kPa did not result in

markedly different appearance of the contractile apparatus. Such elasticity independent behavior is in contrast to results reported for many other cell types: fibroblasts as well as endothelial cells, for example, respond to increasing substrate elasticities with reinforcement processes of cytoskeletal stress fibers as well as adhesion structures (Goffin et al., 2006). Furthermore, several cell types as stem cells or cardiac fibroblasts differentiate in a substrate elasticity dependent manner with prominent changes in almost all types of cytoskeletal and adhesion structures (Engler et al., 2004; Engler et al., 2006; Gilbert et al., 2010).

At this moment we can only speculate about the reason for this constant behavior of myocytes. Since we have used late embryonic rat myocytes (d19) most isolated cells are already partially differentiated and able to contract spontaneously as single cells. Beating itself is a mechanical signal that has been shown to stimulate further muscle cell differentiation and myofibril formation (Damon et al., 2009; Miller et al., 2000). It might therefore be possible that myocytes beyond a certain differentiation state generate their own mechanical late differentiation signal causing the observed elasticity independent myofibril formation. Such a behavior would be physiologically advantageous. In the myocard cardiomyocytes are permanently formed, although at low rates, by differentiation of tissue embedded precursor cells. This happens throughout the whole lifetime of the organism. Because on one hand cardiomyocyte function critically depends on the structure of their force producing apparatus and, on the other hand, myocard stiffness varies enormously during aging or disease progression, myofibril formation should not depend on environmental stiffness. However, it needs to be mentioned that published results on substrate elasticity dependent functional and morphological adaptations of cardiomyocytes are inconsistent to some extent (Bajaj et al., 2010; Bhana et al., 2010; Engler et al., 2008; Jacot et al., 2008; Shi et al., 2011). It might well be that species of origin, exact time point of isolation and even the chemical nature of the cell culture substrate have unexpectedly strong impact.

If plated on soft substrates, contractile forces of our cardiomyocytes were very low. This result is in very good agreement with various other studies (Engler et al., 2008; Jacot et al., 2008). With increasing substrate elasticities contractile cell forces rose. Force values did not peak at a distinct elasticity but instead gradually increased. This behavior resulted in \sim 80 times higher contractile forces on 500 kPa substrates compared to very soft \sim 1 kPa ones. Even for the more natural elasticity range between 15 and 90 kPa this increase was still \sim 4-fold. This almost linear behavior is in marked contrast with non-monotonic behavior reported by Engler and co-workers and Jacot and co-workers, who found a maximum of forces at close to nature substrate elasticity (Engler et al., 2008; Jacot et al., 2008). A probable reason for this contrast is that their cells were isolated at much earlier stages of embryonic development compared to ours. Cardiomyocytes isolated at identical developmental state generated highly comparable contractile forces when tested on 12 kPa substrates (Balaban et al., 2001). Possibly due to the electrical stimulation performed in experiments by Jacot and co-workers, forces generated by single myocytes reported by them (Jacot et al., 2008) were higher on very soft substrates while comparable to our results on stiffer ones.

Interestingly, with values in the range of 3 to 10 μ N overall forces reported for isolated skinned myocytes are much higher

(Diffie and Chung, 2003; Korte and McDonald, 2007) than the highest contractile force of $1 \mu\text{N}$ observed here on stiff substrates. This discrepancy is most likely due to several aspects. Most importantly, effective Ca^{2+} concentrations available to induce myosin activity are clearly different and optimal for skinned cells causing maximum contractions in those cells. Furthermore, cardiomyocytes used for skinned cell preparations are usually isolated from adult, fully differentiated

myocardial tissues. Such cardiomyocytes are characterized by well-aligned myofibrils spanning the whole cell in a defined direction and are therefore different from the prenatal cardiomyocytes used here. Finally, traction force microscopy is not well suited to determine the highest possible contraction forces of cardiomyocytes. These forces are reached under isometric conditions where the contraction amplitude vanishes. While this situation might be approached using very stiff substrates, the resulting tiny substrate deformations cannot be detected anymore.

In addition to forces, we also calculated the work performed by myocytes during one contraction according to Butler and co-workers (Butler et al., 2002). However, a very high scatter of the resulting values (about 1 to 5 fJ) masked all possible dependence on substrate stiffness.

Our results point at the elasticity independent presence and function of myofibrils as reason for the continuous force increase with substrate stiffening. These fibrils are already present in rat cardiomyocytes isolated at day 19 of embryonic development. Subsequent incubation on any substrate elasticity used here had no significant effect on morphology or function of this force generating structure. Although primary cardiomyocytes are by nature a highly heterogeneous cell pool and, additionally, our functional analyses were performed on the mechanically most active subfraction, we noted no dependence of the overall number of myocytes or the number of spontaneously contracting cells on substrate elasticity. Substrate elasticity dependent beat frequency analyses as done elsewhere (Bajaj et al., 2010; Engler et al., 2008) were not performed here due to the naturally high differences of contraction rates between cardiomyocyte subtypes (Joyner et al., 2007; Watanabe et al., 1983).

The only morphological difference that occurred only on the very softest substrates was a more roundish shape of myocytes with possibly slightly less aligned myofibrils. This phenotype is most likely caused directly by low cell force generation on these substrates. Bischofs and co-workers developed a theoretical model that describes the relation between cell shape and cell force distribution based on outer adhesion sites and connecting inward curved actin arcs (Bischofs et al., 2009). Softer substrates result in smaller forces and therefore, according to this model, in less curvature. Consequently, reduction of outer adhesion sites with connecting actin bundles as given for our cardiomyocytes on very soft substrates (Fig. 4B) should result in rounded cell shapes. The slightly reduced order of myofibrils on very soft substrates fits very well with current knowledge. In independent papers Engler and co-workers and Bajaj and co-workers showed similar results for cardiomyocytes grown on very soft polyacrylamide gels (Bajaj et al., 2010; Engler et al., 2008).

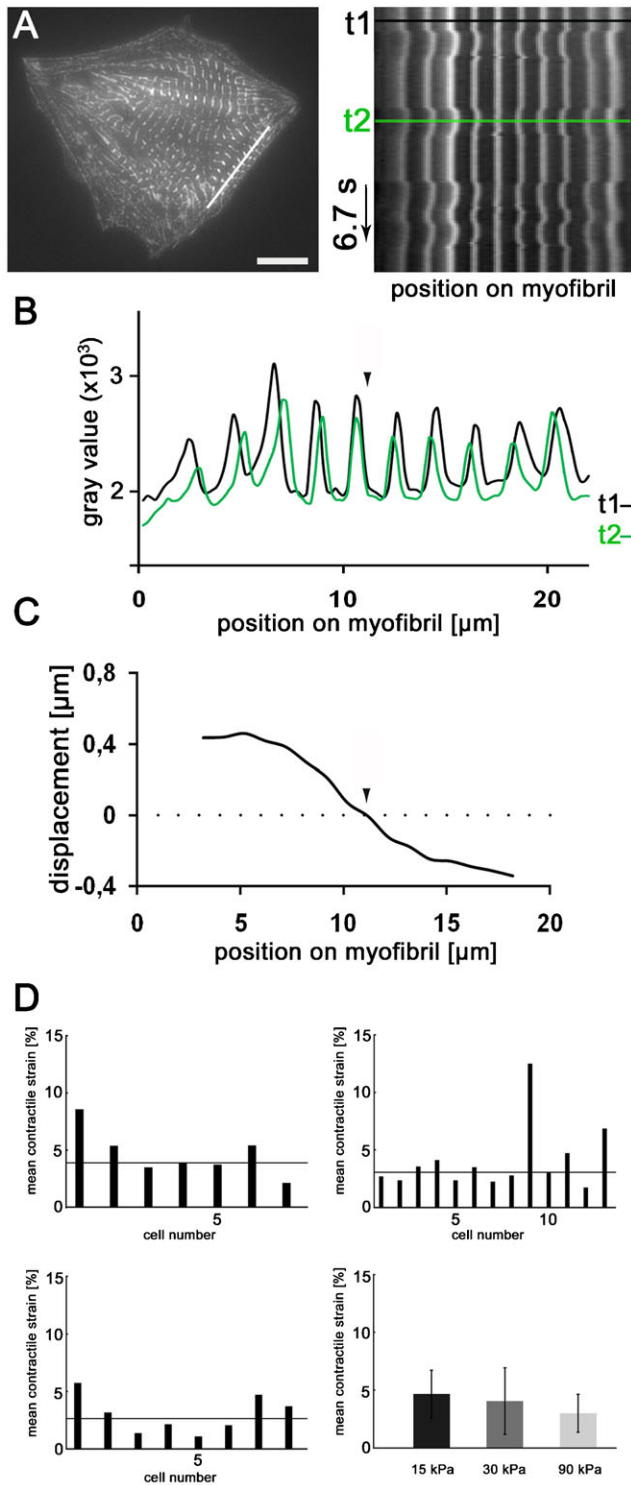


Fig. 8. Constant sarcomeric contractile strain upon substrate stiffening. Contraction of individual myofibrils of GFP- α -actinin transfected cells was analyzed over time along a line spanning their full length (A, left) and plotted as time-space plot (A, right; black arrow indicates direction of time). Scale bar: 10 μm . Gray values along the myofibril at relaxed (t1) and contracted state (t2) show displacements towards the center (black arrowhead in B,C) of the myofibril and enable calculation of displacements of z-bands along the myofibril (C). Note the almost linear dependence of displacement on position in the inner half of the myofibril. Fitted lines characterizing the linear displacement section were averaged over 2–4 independent myofibrils per cell. The resulting slopes (D) describe the average myofibril contractility of each cell on 15 kPa substrates ($n=7$), 30 kPa ($n=13$) and 90 kPa ($n=8$). Mean contractile myofibril strain averaged over all cells per elasticity is given as straight line and separately in (D), bottom right, with included s.d.

Although generated force values increase drastically with substrate stiffening, not only myofibril structure, but also their contractility, seem to be basically unaffected by elasticity within the natural range of 15 to 90 kPa. Our quantitative analyses of myofibril contraction (cf. Fig. 8) revealed relatively stable strain values of about 4% for centrally localized sarcomeres. A possible tendency of reduced contractions on stiffer substrates was not significant and even if it were, this behavior would indicate that cardiomyocytes generate elevating force values on stiffer substrates with even less contraction.

Measurements of sarcomere lengths during single myofibril contractions (e.g. Fig. 8) very clearly showed different behavior in the middle and at the ends of myofibrils. While centrally located sarcomeres contracted, the outer ones were moved at constant length. From basic mechanics this is a very surprising finding because along the myofibril forces must add up resulting in the highest tensile stress at the center of the fibril. At the same time traction forces transmitted by costameres from the elastic substrate to the myofibril were indeed low at the center and increased towards fiber ends (e.g. Fig. 7). Exactly the same behavior is found in technical mechanics for fibers of finite length embedded in a strained elastic matrix (Hsueh, 1989). As sarcomeric lengths were in the range of 1.9 μm where in tissue sarcomere length raises with applied stress a passive material should display contraction mostly at the ends and less in the middle. Taken together basic mechanics and our observations can only be reconciled by assuming that in our experiments individual sarcomeres can sustain the same force at a whole range of lengths. In turn, such a behavior would also imply that sarcomeres at stable length are able to generate a range of forces as we could clearly identify in our experiments (Fig. 8).

At first such a material behavior appears highly implausible. However, it should be seen in the context of the well-studied spontaneous oscillations of isolated myofibrils (Fabiato and Fabiato, 1978; Linke et al., 1993). In this system spontaneous oscillations of sarcomeric lengths and even traveling density waves occur at intermediate levels of excitation, which lead to the same conclusion as presented above (Anazawa et al., 1992). As we observed spontaneous contractions in isolated cells excitation of the contractile system by cellular calcium oscillations was also merely at an intermediate level.

In the abovementioned experiments on isolated myofibrils all sarcomeres within the fibril experience the same force and identical conditions. This is contrary to our case where traction forces transferred from the substrate to the fibril grow towards the ends while tension in the fibril is maximal at center. This could explain why we observed neither travelling waves nor oscillations. In addition, since tensile stress within the myofibril and traction forces transmitted by costameres counteract, relatively small alterations in composition and structure might be sufficient to modify the contractile behavior of myofibrils of isolated cardiomyocytes. Evidence for such small differences between centrally and distally located costameres was found *in vivo* (Bennett et al., 2006; Bennett, 2012) as well as *in vitro* (Goncharova et al., 1992; Sanger et al., 2005; Simpson et al., 1993). Taken together, suboptimal levels of excitation and gradual stress transfer from the substrate, perhaps together with slight variations of myofibril composition towards their ends, are sufficient to reconcile our observations with present knowledge on myofibril contractility.

The model above includes cell adhesion all along the contractile apparatus, which is well supported by our traction force experiments. Here, costameric and focal adhesions equally participate in force transmission, especially on stiff substrates. Only the very central sarcomere units show a clear contractility. Unfortunately, finding a clear correlation between contractile length of myofibrils and substrate stiffness over all substrate elasticities analyzed here was not possible due to limited numbers of analyzable myofibrils of sufficient length. Such experiments were out of the scope of this work due to the very low transfection rates achieved for cardiomyocytes but could finally prove or disprove our model in the future.

Most importantly our data argue for a force generating apparatus in cardiomyocytes achieving stable contraction amplitudes on varying substrate elasticities. Uncoupling cardiomyocytes from surrounding tissue tension leads to stable sarcomere lengths on physiological substrate elasticities between 15 and 90 kPa. Substrate stiffening sarcomeres have to generate higher forces in order to keep their contraction value, which again argues for a force generating machinery never working at full load on soft substrates. Such a regulatory mechanism would therefore be an ideal system to respond instantaneously to environmental changes or just stress factors causing temporal tissue stiffening connected with the necessity of enhanced force values. Sarcomere length regulation as described by the Frank–Starling mechanism in stiffer myocard, will certainly additionally elevate forces generated by myocytes but is not the crucial factor for the force adaptation observed here.

Materials and Methods

Isolation of rat myocytes and myofibroblasts

Cardiomyocytes and cardiac fibroblasts were simultaneously isolated from 19-day-old Wistar rat embryos. Pregnant rats were CO₂ anesthetized and decapitated. The pups were removed and also decapitated under sterile conditions. The heart of each embryo was quickly isolated, washed in Hank's balanced salt solution (HBSS, Sigma, St. Louis, USA), cut into small pieces and digested in 8 ml of a 0.5% Trypsin/0.2% EDTA solution in HBSS to disintegrate the tissue. The supernatant was discarded and resulting cell aggregates were incubated with 100 μl DNase solution (10,000 U/ml, Sigma, St. Louis, USA) for 3 minutes and then filled with 8 ml of TE solution for further 5 minutes. While cell aggregates precipitated without centrifugation, disintegrated single cells remained in the supernatant and were transferred into TE-blocking solution (F10 Ham's medium supplemented with 33% fetal bovine serum). The disintegration step and DNase treatment was repeated one to two more times and supernatants were combined. Cells were then collected by centrifugation at 200 g, maintained at 37°C and 5% CO₂ in a humidified incubator and cultured in F10 Ham's medium supplemented with 10% fetal bovine serum, a 1:100 dilution of an antibiotic solution (10,000 units penicillin and 10 mg/ml streptomycin in 0.9% NaCl, Sigma) and a 1:200 dilution of solution containing insulin (1 mg/ml), transferrin (0.55 mg/ml), and sodium selenite (0.5 $\mu\text{g}/\text{ml}$) in EBSS (Sigma, St. Louis, USA). Myocytes were seeded on fibronectin (2.5 $\mu\text{g}/\text{cm}^2$) (BD Biosciences, San Jose, CA) coated cross-linked silicone rubber substrates of diverse and controlled elasticities.

For some experiments cardiac fibroblasts were cultured for additional 3 days on standard polystyrene cell culture dishes in supplemented F10 Ham's medium to induce their differentiation to myofibroblasts. Differentiated cells were trypsinized and used for control experiments as described below.

Cell transfection

Cardiomyocytes and myofibroblasts were transfected using Nucleofector technology (Lonza–Amaxa Biosystems, Cologne, Germany). 2×10^6 cells were resuspended in 100 μl Nucleofector solution. 2 μg purified plasmid-DNA (GFP- α -actinin for myocytes and GFP-VASP for myofibroblasts) was added to the sample and cells were transfected according to the manufacturer's instructions (program G09). Transfection rates ranged between 0.1 and 1% for cardiomyocytes and were ~5% for myofibroblasts. After transfection, resuspended cells were seeded on fibronectin coated cross-linked silicone rubber substrates at a cell density of $2\text{--}4 \times 10^4$ per Petri dish (ϕ 3.5 cm).

Fabrication of silicone rubber substrates

For cell force analysis of cardiomyocytes, cells were seeded on cross-linked elastomeric silicone rubber substrates (*Sylgard 184*, Dow Corning GmbH). Substrate preparation and characterization of elastomer material properties (Young's modulus and Poisson's ratio) were performed as described previously (Cesa et al., 2007). In brief, various ratios (see below) of base (vinyl terminated polydimethylsiloxane) and cross-linker (methylhydrosiloxane–dimethylsiloxane copolymer) were prepared. The prepolymer mixtures were degassed and one part of the mixture was mixed with red fluorescent beads (0.2 μm diameter, FluoSpheres Crimson carboxylate-modified beads, Invitrogen) and subsequently applied on a previously silanized (1H, 1H', 2H, 2H'-perfluorooctyl-trichlorosilane, Sigma) micro-structured silicon dioxide mold. The microstructure was composed of a square lattice consisting of 500 nm high microdots with an edge length of 2.5 μm and a lattice constant of 3.5 μm . The layer thickness of the fluorescent bead/prepolymer mixture was reduced to less than 500 nm by wiping the surface with lint-free tissue. The remaining non-cross-linked prepolymer lacking fluorescent beads was added on top of the thin fluorescent bead/prepolymer layer. Glass slides (80 μm thick, Menzel GmbH, Germany) served as spacers and were placed on the silicone mixture beside the microstructure. Subsequently, they were covered with an additional 80 μm coverslip on top to obtain a constant layer thickness. Cross-linking was performed at 60°C overnight. Elastomeric substrates were subsequently glued to the bottom of 3.5 cm Petri dishes to cover predrilled 1.5 cm holes. After curing, these silicone rubbers displayed a Poisson's ratio of 0.5 and a Young's modulus of 500 kPa (20:1 ratio; base to cross-linker w/w), 150 kPa (30:1), 90 kPa (35:1), 30 kPa (45:1), 15 kPa (50:1) and \sim 1 kPa (70:1). The elasticity for the very soft \sim 1 kPa substrates could not be accurately analyzed due to their softness and stickiness. Therefore, the elasticity of those substrates was estimated by extrapolating existing calibrations.

Microscopy

Live cell analyses were performed at 37°C and 5% CO₂ (cell incubator XL2, Zeiss, Germany) using an inverted microscope (Axiovert 200, Zeiss, Germany), equipped with a CCD camera (Orca black-and-white, Hamamatsu, Japan) utilizing a 63 \times Antiflex EC Plan-Neofluar oil immersion objective (PH3, NA=1.25, Zeiss, Germany). Images were taken using the imaging software OpenBox (version 1.77, Informationssysteme Schilling, Germany). Excitation of GFP- α -actinin and of fluorescent beads was done with a mercury arc lamp (HBO 100, Osram, Germany). Fluorescent images of GFP- α -actinin were obtained using a 505–530 nm bandpass filter, for the fluorescent beads a 590 nm long-pass filter was used.

Immunofluorescently labeled cells were analyzed with an inverse confocal laser scanning microscope (LSM 710, Zeiss, Germany) using a 40 \times Plan-Neofluar oil immersion objective (Ph3, NA 1.3, Zeiss, Germany) and a 63 \times Plan-Apochromat oil immersion objective (Ph3, NA 1.4, Zeiss, Germany). Confocal micrographs were taken using an argon ion laser (488 nm) with a 490–530 nm bandpass filter and a helium–neon laser (543 nm) with a 550–812 nm bandpass filter.

Immunofluorescence techniques

Myocytes (3 \times 10⁴ cells per substrate) were seeded on silicone rubber substrates with different stiffness ranging from \sim 1 to 500 kPa and stained after 3 days. Myocytes were fixed using 3.7% formaldehyde (Merck, Germany) in cytoskeleton buffer (CB: 150 mM NaCl, 5 mM MgCl₂, 5 mM EGTA, 5 mM glucose, 1 mg/ml streptomycin, 10 mM MES, pH 6.1) for 20 minutes at 37°C. Subsequently, cells were washed once with 30 mM glycine in CB for 10 minutes, permeabilized with 5% Triton X-100 (Sigma, St. Louis, USA) in CB for 3 minutes at room temperature, rinsed twice with CB and then treated with blocking solution (5% skim milk powder (Sigma) in CB) for 45 minutes at 37°C. Primary antibodies (anti-vinculin, clone hVin-1 (Sigma, St. Louis, USA); anti- α -actinin, clone EA 53 (Sigma, St. Louis, USA); anti-plectin, clone 10F6 (Santa Cruz Biotechnology, Santa Cruz, CA) and secondary antibodies conjugated to Cy3 (Dianova, Hamburg, Germany) were both diluted 1:100 in 1% skim milk powder in CB and applied each for 45 minutes at 37°C with three additional washing steps with CB between the primary and secondary antibody. For actin staining Alexa Fluor488 phalloidin (Invitrogen, Carlsbad, USA) was used in a 1:200 dilution in CB together with the secondary antibody for 45 minutes at 37°C.

Cell shape determination

For quantifying cell roundness we used a dimensionless shape index si defined as $si = 4\pi AP^{-2}$ where A denotes the area of the cell and P its perimeter. For any shape si is in between 1 (circle) and 0 (line). For calculating si the shape of a cell was approximated by a polygon with interactively chosen corner points (depending on cell shape typically between 20 and 40). Cells exhibiting si above 0.8 were classified as round, all others as angular.

Detection of GFP- α -actinin clusters in micrographs

Fluorescence micrographs of cells transfected with GFP- α -actinin exhibited bright clusters indicating FAs and z-bands. For the localization of these clusters a

segmentation routine was developed. It started with bandpass filtering of the images by subtracting two binomially filtered images (9 \times 9 binomial filtered minus 57 \times 57 binomial filtered). Pixel size was 0.2 μm . Subsequently, for each pixel of this preprocessed image local average and local standard deviation were calculated within a 91 \times 91 environment. These values were used to replace each pixel value by the z-score, i.e. the local average was subtracted and the result normalized by the local standard deviation. All connected regions exceeding a threshold size (usually 10 pixels) and a threshold z-score (usually 0.7) were classified as clusters.

In some micrographs highly elongated and obviously artificial clusters were identified by this routine. These artifacts were removed by the following criterion. For each cluster the ellipse with equal central second moments was calculated. The distribution of the semi-major axes of these ellipses was transformed into the z-score (definition see above). All areas exceeding an interactively chosen threshold value (typically 15) were considered artifacts and removed. From the remaining data we calculated average cluster size, the number of clusters within a given cell and the fraction of the cell area covered by clusters. To this end cell areas were interactively marked by polygons as above.

Cell force retrieval

Traction forces applied by the cell to the elastic substrate caused substrate deformations that were visualized by tracking fluorescent marker beads in the uppermost layer of the substrate (see above). From the displacements of these particles cell forces were calculated. These calculations are based on the very well understood behavior of layered elastic materials in response to external forces (cf. Merkel et al., 2007; and references therein). The specific silicone elastomer system used here has been shown to fulfill the prerequisites of the above mentioned theory, i.e. they are homogeneous and isotropic media exhibiting linear elasticity up to very large extensions (Balaban et al., 2001; Cesa et al., 2007; Gutierrez and Groisman, 2011). However, for rapidly contracting cells like cardiomyocytes viscoelastic material behavior is a concern, especially for the softest rubbers. We therefore measured the force relaxation after a rapid indentation step (0.2 second) with a cylindrical punch. The ratio of force after the duration of an average contraction (\sim 0.3 second) and at very long times was 2.1 for the very softest rubber (\sim 1 kPa) and 1.3 for 15 kPa rubber. As stiffer elastomers exhibit faster force relaxation and the overall accuracy of the technique is about 30%, we concluded that viscoelastic material behavior plays a significant role for the softest elastomer only.

Moreover, for isolated cells of the size of myocytes a layer of 80 μm thickness behaves almost exactly like an elastic half space (Merkel et al., 2007). This greatly simplifies the underlying mathematics and enabled us to use the analytical expressions derived first by Boussinesq (Boussinesq, 1885). These expressions correctly describe the displacements caused by a point force acting on the surface of the elastomer. Our algorithms (see below) assume a test force distribution, calculate the cumulative displacement caused by all these forces and iteratively improve the force distribution until it reproduces the measured displacements. Unfortunately, in traction force microscopy this conceptually straightforward approach involves some less than intuitive methods of numerical mathematics. For details see e.g. Merkel and co-workers and Schwarz and co-workers (Merkel et al., 2007; Schwarz et al., 2002). Our implementation works as described below.

Bead displacements were first determined as described by Merkel and co-workers (Merkel et al., 2007). In short, the first image of the sequence was used as reference image. A small region around a randomly chosen microbead was used as template. All other beads were localized by cross-correlating this template with the image and finding local maxima of the normalized correlation coefficient with sub-pixel accuracy. Only places where the normalized cross-correlation coefficient exceeded a threshold value (typically 0.8) were accepted as bead positions. In subsequent frames microbeads were localized using bead-specific templates and their displacements with respect to the reference image were calculated with an accuracy of 25 nm.

Force retrieval from these displacements is more complicated as mathematically the displacement vector field originates from the force field by a convolution with a stiffness dependent Greens' tensor that exhibits a singularity at the origin and decays as one over distance. Inverting this convolution is a numerically ill-posed problem requiring regularized least squares fit or related algorithms (Dembo and Wang, 1999; Merkel et al., 2007; Schwarz et al., 2002).

In this work we used two different algorithms. One is based on a superposition of optimally chosen point forces localized at manually predefined locations (cell adhesion sites), the other calculates entire force fields. The point force algorithm was developed by Schwarz and co-workers and used as described by Cesa and co-workers (Schwarz et al., 2002; Cesa et al., 2007). The force field algorithm used is described in detail by Houben and co-workers (Houben et al., 2010). Both algorithms yield force distributions. To assess the quality of these solutions we calculated the displacements resulting from the retrieved force distribution and compared it with the measured bead displacements. Besides a visual comparison we calculated the normalized squared deviation, χ^2 , between fit result and measured data according to $\chi^2 = [2(N_B - N_F)\sigma^2]^{-1} \sum_{i=1}^{N_B} (\bar{u}_{Bi} - \bar{u}_{Fi})^2$ where N_B signifies the total number of tracked beads with displacements \bar{u}_{Bi} (measured) and \bar{u}_{Fi} (calculated). N_F is the total number of force induction points and σ the standard deviation of displacement measurement (here 25 nm).

For the characterization of cell contractions we calculated the sum of all contractile forces. For the point force algorithm we proceeded as described by Merkel and co-workers (Merkel et al., 2007). Here, force application points were chosen on a regular hexagonal grid (lattice constant 5 μm) covering the whole cell area. Subsequently, the cell center was calculated as the center of gravity of these points. The contractile parts of all forces, i.e. the force components pointing towards the cell center, were summed up to yield the total contractile force. This procedure enables the calculation of overall cell contraction force values although according to Newton's principles all force vectors here and for any other stably adhered cell sum up to zero.

In the other case, the force field algorithm, the whole micrograph is covered by a mesh comprising almost the same number of vertices as beads were tracked (typically 2,000–4,000). Forces are calculated at each vertex. Therefore we could calculate the contractile force in almost the same way as before. In effect the geometrical center of the cell was determined and within the cell area the contractile parts of all forces were added.

For some control analyses we performed traction force experiments on GFP-VASP transfected myofibroblasts. Bead microstructured elastomer substrate preparation, bead displacement determination and traction force analyses (point force algorithm) were performed as described above for cardiomyocytes. In order to obtain a reference image of the non-deformed substrate beneath the analyzed cells, myofibroblasts were removed manually from the substrate using a glass micropipette mounted on a microinjector (Inject Man N12, Eppendorf, Germany). As force induction points we either used FAs labeled by GFP-VASP or an interactively chosen lattice of $\sim 4 \mu\text{m}$ spacing beneath the central cell body to mimic adhesion sites along myofibrils of cardiomyocytes.

High-resolution myofibril contraction analysis

Fluorescent micrographs of cells transfected with GFP- α -actinin clearly showed a sarcomere structure. Due to the corresponding brightness variation along the fibril contractions could be accurately quantified by image correlation. In detail we proceeded as follows. The image was denoised with a 3×3 binomial filter (pixel size 0.2 μm). Subsequently, a myofibril was traced with connecting straight lines. At distances closely corresponding to the original pixel size gray values were determined by interpolation from the neighboring pixels. In the following we will refer to the resulting vector as "profile". Gray value extraction was repeated for each image of the sequence along the same line. In the results section these profiles are shown in the space-time plane. Such plots are sometimes also called kymographs.

Before the actual calculation of sarcomere displacements each profile was again smoothed by a binomial filter of width 3. The first profile of a sequence was used as reference. It was subdivided into overlapping templates. Spacing between template centers was 5 pixels, template width was chosen typically between 15 and 25 pixels. At each later time point displacements along the myofibril were found by cross-correlating each template with the respective profile. Sub-pixel resolution was achieved by fitting a parabola to the maxima of the cross-correlation coefficient and determining its symmetry point. This procedure yielded displacement profiles with one displacement value every five pixels. For each contraction of the myofibril the time point of the maximum displacement was found. Displacement profiles at maximum contractions (typically five) were averaged and further analyzed.

To determine the central slope of these averaged displacement profiles we first determined the useful fit range. This was taken to be the range between the numerically determined inflection points of the displacement profile. In the actual experiments this region was 5 to 10 μm wide. Within this range a straight line was fitted to the data. Its slope corresponds to the contractile strain (relative shortening) of the myofibril in its center region. Subsequently, the contractile strain values of all evaluated myofibrils within a cell (mostly two to four) were averaged.

Acknowledgements

We thank W. Rubner for helpful discussions and expert technical support. We also thank E. Noetzel for critical reading of the manuscript and T. Jonas for cell isolation and helpful discussions. This work was supported by the German Bundesministerium für Bildung und Forschung (BMBF, project title: MechanoSys, BMBF-Nr. 0315501A).

Competing Interests

The authors have no competing interests to declare.

References

Anazawa, T., Yasuda, K. and Ishiwata, S. (1992). Spontaneous oscillation of tension and sarcomere length in skeletal myofibrils. Microscopic measurement and analysis. *Biophys. J.* **61**, 1099–1108.

- Bajaj, P., Tang, X., Saif, T. A. and Bashir, R. (2010). Stiffness of the substrate influences the phenotype of embryonic chicken cardiac myocytes. *J. Biomed. Mater. Res. A* **95A**, 1261–1269.
- Balaban, N. Q., Schwarz, U. S., Riveline, D., Goichberg, P., Tzur, G., Sabanay, I., Mahalu, D., Safran, S., Bershadsky, A., Addadi, L. et al. (2001). Force and focal adhesion assembly: a close relationship studied using elastic micropatterned substrates. *Nat. Cell Biol.* **3**, 466–472.
- Bennett, P. M. (2012). From myofibril to membrane; the transitional junction at the intercalated disc. *Front. Biosci.* **17**, 1035–1050.
- Bennett, P. M., Maggs, A. M., Baines, A. J. and Pinder, J. C. (2006). The transitional junction: a new functional subcellular domain at the intercalated disc. *Mol. Biol. Cell* **17**, 2091–2100.
- Berry, M. F., Engler, A. J., Woo, Y. J., Pirolli, T. J., Bish, L. T., Jayasankar, V., Morine, K. J., Gardner, T. J., Discher, D. E. and Sweeney, H. L. (2006). Mesenchymal stem cell injection after myocardial infarction improves myocardial compliance. *Am. J. Physiol. Heart Circ. Physiol.* **290**, H2196–H2203.
- Bhana, B., Iyer, R. K., Chen, W. L. K., Zhao, R., Sider, K. L., Likhitpanichkul, M., Simmons, C. A. and Radisic, M. (2010). Influence of substrate stiffness on the phenotype of heart cells. *Biotechnol. Bioeng.* **105**, 1148–1160.
- Bischofs, I. B., Schmidt, S. S. and Schwarz, U. S. (2009). Effect of adhesion geometry and rigidity on cellular force distributions. *Phys. Rev. Lett.* **103**, 048101.
- Boussinesq, J. (1885). *Application Des Potentiels À L'étude De L'équilibre Et Du Mouvement Des Solides Élastiques*. Paris: Gauthier-Villars.
- Butler, J. P., Tolić-Nørrelykke, I. M., Fabry, B. and Fredberg, J. J. (2002). Traction fields, moments, and strain energy that cells exert on their surroundings. *Am. J. Physiol. Cell Physiol.* **282**, C595–C605.
- Cesa, C. M., Kirchgessner, N., Mayer, D., Schwarz, U. S., Hoffmann, B. and Merkel, R. (2007). Micropatterned silicone elastomer substrates for high resolution analysis of cellular force patterns. *Rev. Sci. Instrum.* **78**, 034301.
- Damon, B. J., Rémond, M. C., Bigelow, M. R., Trusk, T. C., Xie, W., Perucchio, R., Sedmera, D., Denslow, S. and Thompson, R. P. (2009). Patterns of muscular strain in the embryonic heart wall. *Dev. Dyn.* **238**, 1535–1546.
- Danowski, B. A., Imanaka-Yoshida, K., Sanger, J. M. and Sanger, J. W. (1992). Costameres are sites of force transmission to the substratum in adult rat cardiomyocytes. *J. Cell Biol.* **118**, 1411–1420.
- de Tombe, P. P., Mateja, R. D., Tachampa, K., Ait Mou, Y., Farman, G. P. and Irving, T. C. (2010). Myofilament length dependent activation. *J. Mol. Cell. Cardiol.* **48**, 851–858.
- Decker, M. L., Simpson, D. G., Behnke, M., Cook, M. G. and Decker, R. S. (1990). Morphological analysis of contracting and quiescent adult rabbit cardiac myocytes in long-term culture. *Anat. Rec.* **227**, 285–299.
- Dembo, M. and Wang, Y. L. (1999). Stresses at the cell-to-substrate interface during locomotion of fibroblasts. *Biophys. J.* **76**, 2307–2316.
- Diffie, G. M. and Chung, E. (2003). Altered single cell force-velocity and power properties in exercise-trained rat myocardium. *J. Appl. Physiol.* **94**, 1941–1948.
- Discher, D. E., Mooney, D. J. and Zandstra, P. W. (2009). Growth factors, matrices, and forces combine and control stem cells. *Science* **324**, 1673–1677.
- Du, A., Sanger, J. M., Linask, K. K. and Sanger, J. W. (2003). Myofibrillogenesis in the first cardiomyocytes formed from isolated quail precardiac mesoderm. *Dev. Biol.* **257**, 382–394.
- Engler, A. J., Griffin, M. A., Sen, S., Bönnemann, C. G., Sweeney, H. L. and Discher, D. E. (2004). Myotubes differentiate optimally on substrates with tissue-like stiffness: pathological implications for soft or stiff microenvironments. *J. Cell Biol.* **166**, 877–887.
- Engler, A. J., Sen, S., Sweeney, H. L. and Discher, D. E. (2006). Matrix elasticity directs stem cell lineage specification. *Cell* **126**, 677–689.
- Engler, A. J., Carag-Krieger, C., Johnson, C. P., Raab, M., Tang, H. Y., Speicher, D. W., Sanger, J. W., Sanger, J. M. and Discher, D. E. (2008). Embryonic cardiomyocytes beat best on a matrix with heart-like elasticity: scar-like rigidity inhibits beating. *J. Cell Sci.* **121**, 3794–3802.
- Fabiato, A. and Fabiato, F. (1978). Myofilament-generated tension oscillations during partial calcium activation and activation dependence of the sarcomere length-tension relation of skinned cardiac cells. *J. Gen. Physiol.* **72**, 667–699.
- Fukuda, N., O-Uchi, J., Sasaki, D., Kajiwara, H., Ishiwata, S. and Kurihara, S. (2001). Acidosis or inorganic phosphate enhances the length dependence of tension in rat skinned cardiac muscle. *J. Physiol.* **536**, 153–160.
- Giannone, G., Jiang, G., Sutton, D. H., Critchley, D. R. and Sheetz, M. P. (2003). Talin1 is critical for force-dependent reinforcement of initial integrin-cytoskeleton bonds but not tyrosine kinase activation. *J. Cell Biol.* **163**, 409–419.
- Gilbert, P. M., Havenstrite, K. L., Magnusson, K. E., Sacco, A., Leonardi, N. A., Kraft, P., Nguyen, N. K., Thrun, S., Lutolf, M. P. and Blau, H. M. (2010). Substrate elasticity regulates skeletal muscle stem cell self-renewal in culture. *Science* **329**, 1078–1081.
- Goffin, J. M., Pittet, P., Csucs, G., Lussi, J. W., Meister, J. J. and Hinz, B. (2006). Focal adhesion size controls tension-dependent recruitment of α -smooth muscle actin to stress fibers. *J. Cell Biol.* **172**, 259–268.
- Goncharova, E. J., Kam, Z. and Geiger, B. (1992). The involvement of adherens junction components in myofibrillogenesis in cultured cardiac myocytes. *Development* **114**, 173–183.
- Gupta, K. B., Ratcliffe, M. B., Fallert, M. A., Edmunds, L. H. and Jr and Bogen, D. K. (1994). Changes in passive mechanical stiffness of myocardial tissue with aneurysm formation. *Circulation* **89**, 2315–2326.

- Gutierrez, E. and Groisman, A.** (2011). Measurements of elastic moduli of silicone gel substrates with a microfluidic device. *PLoS ONE* **6**, e25534.
- Hanft, L. M., Korte, F. S. and McDonald, K. S.** (2008). Cardiac function and modulation of sarcomeric function by length. *Cardiovasc. Res.* **77**, 627-636.
- Herrmann, K. L., McCulloch, A. D. and Omens, J. H.** (2003). Glycated collagen cross-linking alters cardiac mechanics in volume-overload hypertrophy. *Am. J. Physiol. Heart Circ. Physiol.* **284**, H1277-H1284.
- Hilenski, L. L., Ma, X. H., Vinson, N., Terracio, L. and Borg, T. K.** (1992). The role of β_1 integrin in spreading and myofibrillogenesis in neonatal rat cardiomyocytes *in vitro*. *Cell Motil. Cytoskeleton* **21**, 87-100.
- Hinz, B.** (2009). Tissue stiffness, latent TGF- β 1 activation, and mechanical signal transduction: implications for the pathogenesis and treatment of fibrosis. *Curr. Rheumatol. Rep.* **11**, 120-126.
- Houben, S., Kirchgessner, N. and Merkel, R.** (2010). Estimating force fields of living cells – comparison of several regularization schemes combined with automatic parameter choice. *Lecture Notes in Computer Science* **6376**, 71-80.
- Hsueh, C. H.** (1989). Analytical analyses of stress transfer in fibre-reinforced composites with bonded and debonded fibre ends. *J. Mater. Sci.* **24**, 4475-4482.
- Jacot, J. G., McCulloch, A. D. and Omens, J. H.** (2008). Substrate stiffness affects the functional maturation of neonatal rat ventricular myocytes. *Biophys. J.* **95**, 3479-3487.
- Jacot, J. G., Martin, J. C. and Hunt, D. L.** (2010). Mechanobiology of cardiomyocyte development. *J. Biomech.* **43**, 93-98.
- Joyner, R. W., Wilders, R. and Wagner, M. B.** (2007). Propagation of pacemaker activity. *Med. Biol. Eng. Comput.* **45**, 177-187.
- Koltai, M. Z., Balogh, I., Wagner, M. and Pogátsa, G.** (1984). Diabetic myocardial alterations in ultrastructure and function. *Exp. Pathol.* **25**, 215-221.
- Konieczny, P., Fuchs, P., Reipert, S., Kunz, W. S., Zeöld, A., Fischer, I., Paulin, D., Schröder, R. and Wiche, G.** (2008). Myofiber integrity depends on desmin network targeting to Z-disks and costameres via distinct plectin isoforms. *J. Cell Biol.* **181**, 667-681.
- Korte, F. S. and McDonald, K. S.** (2007). Sarcomere length dependence of rat skinned cardiac myocyte mechanical properties: dependence on myosin heavy chain. *J. Physiol.* **581**, 725-739.
- Krishnan, R., Park, C. Y., Lin, Y. C., Mead, J., Jaspers, R. T., Trepap, X., Lenormand, G., Tambe, D., Smolensky, A. V., Knoll, A. H. et al.** (2009). Reinforcement versus fluidization in cytoskeletal mechanoresponsiveness. *PLoS ONE* **4**, e5486.
- Linke, W. A., Bartoo, M. L. and Pollack, G. H.** (1993). Spontaneous sarcomeric oscillations at intermediate activation levels in single isolated cardiac myofibrils. *Circ. Res.* **73**, 724-734.
- Martyn, D. A. and Gordon, A. M.** (2001). Influence of length on force and activation-dependent changes in troponin c structure in skinned cardiac and fast skeletal muscle. *Biophys. J.* **80**, 2798-2808.
- Mazhari, R., Omens, J. H., Covell, J. W. and McCulloch, A. D.** (2000). Structural basis of regional dysfunction in acutely ischemic myocardium. *Cardiovasc. Res.* **47**, 284-293.
- Merkel, R., Kirchgessner, N., Cesa, C. M. and Hoffmann, B.** (2007). Cell force microscopy on elastic layers of finite thickness. *Biophys. J.* **93**, 3314-3323.
- Miller, C. E., Donlon, K. J., Toia, L., Wong, C. L. and Chess, P. R.** (2000). Cyclic strain induces proliferation of cultured embryonic heart cells. *In Vitro Cell. Dev. Biol. Anim.* **36**, 633-639.
- Rassier, D. E. and Pavlov, I.** (2010). Contractile characteristics of sarcomeres arranged in series or mechanically isolated from myofibrils. *Adv. Exp. Med. Biol.* **682**, 123-140.
- Rodriguez, A. G., Han, S. J., Regnier, M. and Sniadecki, N. J.** (2011). Substrate stiffness increases twitch power of neonatal cardiomyocytes in correlation with changes in myofibril structure and intracellular calcium. *Biophys. J.* **101**, 2455-2464.
- Sanger, J. W., Kang, S., Siebrands, C. C., Freeman, N., Du, A., Wang, J., Stout, A. L. and Sanger, J. M.** (2005). How to build a myofibril. *J. Muscle Res. Cell Motil.* **26**, 343-354.
- Schwarz, U. S., Balaban, N. Q., Riveline, D., Bershadsky, A., Geiger, B. and Safran, S. A.** (2002). Calculation of forces at focal adhesions from elastic substrate data: the effect of localized force and the need for regularization. *Biophys. J.* **83**, 1380-1394.
- Shapira-Schwartz, K. and Seliktar, D.** (2007). Matrix stiffness affects spontaneous contraction of cardiomyocytes cultured within a PEGylated fibrinogen biomaterial. *Acta Biomater.* **3**, 33-41.
- Sharp, W. W., Simpson, D. G., Borg, T. K., Samarel, A. M. and Terracio, L.** (1997). Mechanical forces regulate focal adhesion and costamere assembly in cardiac myocytes. *Am. J. Physiol.* **273**, H546-H556.
- Shi, X., Qin, L., Zhang, X., He, K., Xiong, C., Fang, J., Fang, X. and Zhang, Y.** (2011). Elasticity of cardiac cells on the polymer substrates with different stiffness: an atomic force microscopy study. *Phys. Chem. Chem. Phys.* **13**, 7540-7545.
- Simpson, D. G., Decker, M. L., Clark, W. A. and Decker, R. S.** (1993). Contractile activity and cell-cell contact regulate myofibrillar organization in cultured cardiac myocytes. *J. Cell Biol.* **123**, 323-336.
- van den Borne, S. W., Diez, J., Blankesteyn, W. M., Verjans, J., Hofstra, L. and Narula, J.** (2010). Myocardial remodeling after infarction: the role of myofibroblasts. *Nat. Rev. Cardiol.* **7**, 30-37.
- Watanabe, T., Delbridge, L. M., Bustamante, J. O. and McDonald, T. F.** (1983). Heterogeneity of the action potential in isolated rat ventricular myocytes and tissue. *Circ. Res.* **52**, 280-290.

Supplementary Material

Nils Hersch et al. doi: 10.1242/bio.20133830

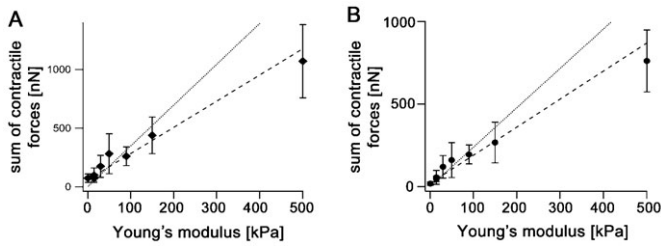
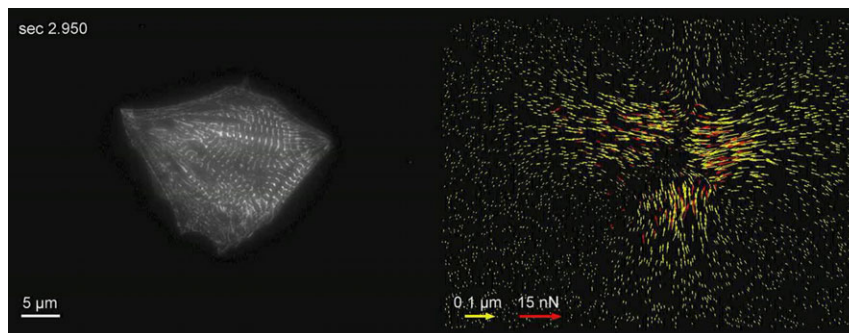


Fig. S1. Maximum values of the sum of all contractile forces were calculated using either the point force algorithm (A, see also Fig. 6D) or the force field algorithm (B, see also Fig. 7D). Subsequently, force values were averaged for all cells per substrate elasticity and plotted with the respective s.d. using a linear substrate stiffness scale. The dotted line displays a fitted proportional force increase while the dashed line indicates a fitted linear force increase.



Movie 1. α -actinin transfected cardiomyocytes were grown on bead microstructured elastomeric substrates. After 3 days cells were successively analyzed in fluorescence for α -actinin localization (left) and bead displacement over time. Subsequently, bead displacements were determined using image processing techniques (yellow arrows, right) and cell forces applied at interactively chosen FAs and costameres were calculated (red arrows, right). The exemplarily presented cell was grown on a 30 kPa stiff substrate. Resolution: 1280×720; frame rate: 59 milliseconds; number of images: 73.